Supplementary material to "Slab Break-offs in the Alpine Subduction Zone"

Emanuel D. Kästle[1], Claudio Rosenberg[2], Lapo Boschi[2,3], Nicolas Bellahsen[2], Thomas Meier[4], and Amr El-Sharkawy[4,5]

[1]Institute of Geological Sciences, Freie Universität Berlin, Germany
[2]Institut des Sciences de la Terre, Paris (iSTeP), Sorbonne Université, Paris, France
[4]Christian Albrechts Universität Kiel, Germany
[3]Dipartimento di Geoscienze, Universita' degli Studi di Padova, Italy
[5]National Research Insititute of Astronomy and Geophysics (NRIAG), 11421, Helwan, Cairo, Egypt

Contents of this file

Introduction The supplementary material gives a side-by-side comparison of the nine tomographic models discussed in the main article in Figures S1–S14, and a summary of the findings on the eastern Alpine slab geometry and amount of shortening in Table S1. Figure S1–S3 show the models in map view at depth levels of 100 km, 200 km and 300 km, Figures S4–S14 show the models along different cross-sections. Not all models cover the entire region. If a model has no resolution at all along a certain section, it is not shown. The color map is the same for all plotted models, however, the color scale is different in order to have the best comparability of the slab geometries. The model based on surface waves (Kästle et al., 2018) and the models based on full-waveform tomography (Zhu et al., 2015; Fichtner et al., 2018) give shear-velocity deviations instead of compressional-velocity deviations. The difference in sensitivity of the velocity types to the structural parameters leads to additional differences shape and strength of the imaged anomalies.

Table S 1: Main observations concerning the subduction in the eastern Alps.

Depth of slab tip (variable along latitude)	$> 400\ km$ (Piromallo and Morelli, 2003) (discontinuous) $\sim 250\ km$ (Lippitsch et al., 2003) $> 400\ km$ (Koulakov et al., 2009) $> 400\ km$ (Dando et al., 2011) $> 400\ km$ (Mitterbauer et al., 2011) $> 400\ km$ (Zhu et al., 2015) $> 400\ km$ (Zhao et al., 2016) $> 400\ km$ (Hua et al., 2017) (discontinuous) $200 - 300\ km$ (Fichtner et al., 2018)
Slab dip	All body-wave tomographic models show a vertical to subvertical, slightly northward dipping slab between 12° and 14° longitude, if the anomaly geometry is averaged over the entire depth range (Lippitsch et al., 2003; Koulakov et al., 2009; Dando et al., 2011; Mitterbauer et al., 2011; Zhu et al., 2015; Zhao et al., 2016; Hua et al., 2017).
E-W slab continuity	All models show a gap or discontinuity (northward step) between central and eastern Alpine anomalies (Piromallo and Morelli, 2003; Lippitsch et al., 2003; Koulakov et al., 2009; Mitterbauer et al., 2011; Zhao et al., 2016; Hua et al., 2017).
Vertical slab continuity	Lippitsch et al. (2003) show a slab that is continuous from the lithosphere down to 250 km depth. Other authors show a rather continuous slab down to the mantle transition zones (Koulakov et al., 2009; Dando et al., 2011; Mitterbauer et al., 2011; Zhu et al., 2015; Zhao et al., 2016). Anomaly variations in vertical direction are not interpreted by the authors. The images by Hua et al. (2017) and Fichtner et al. (2018) show a significantly weakened anomaly in the upper 200 km. A slab window between 100–200 km is also indicated in the model of Piromallo and Morelli (2003). All models that cover areas east of 14°E indicate that the slab anomaly weakens and then disappears in the upper 250 km (Piromallo and Morelli, 2003; Koulakov et al., 2009; Dando et al., 2011; Mitterbauer et al., 2011; Zhu et al., 2015; Zhao et al., 2016; Hua et al., 2017; Fichtner et al., 2018).
N-S shortening	Total of 190 km, mostly in the southern Alps (Ustaszewski et al., 2008) minimum 55 – 75 km in the southern Alps (Brückl, 2011) minimum 50 km in the southern Alps (Schönborn, 1999; Nussbaum, 2000)
Moho offset	An offset suggesting that Europe is the lower plate is imaged along the TRANSALP cross-section in the work of Kummerow et al. (2004). This may be due to indentation of Adria at mid-crustal levels. More recent results suggest rather that the Moho structure is ambiguous in this area (e.g., Spada et al., 2013). Hetényi et al. (2018) confirm the ambiguity of Moho structure in this area but find indications of deeper Adriatic Moho.

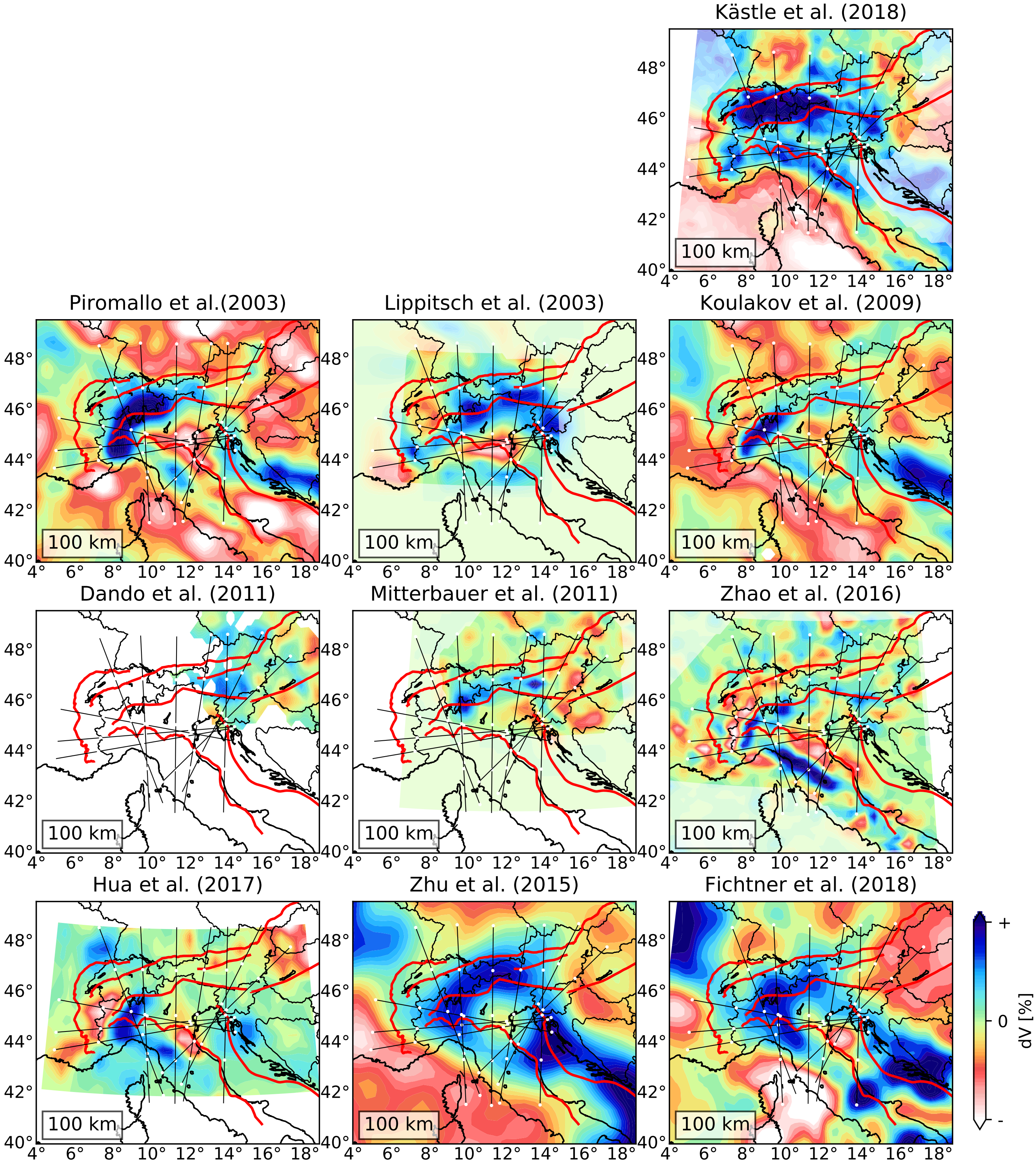

Figure S 1: Map comparison of different tomographic models at 100 km depth. The colors show either shear-velocity deviations (Zhu et al., 2015; Kästle et al., 2018; Fichtner et al., 2018) or compressional-velocity deviations (other models) from a regional starting model. The color scale is normalized to ±5% for Lippitsch et al. (2003); Zhu et al. (2015); Fichtner et al. (2018), ±4% for (Zhao et al., 2016), ±2.5 for Kästle et al. (2018) and ±3% for the other models. In most models, only central parts of the shown region are well resolved. Faults and tectonic limits (red lines) simplified from Schmid et al. (2004, 2008); Handy et al. (2010). Lighter colors indicate regions of lower resolution as defined in the original works. For an explanation of the abbreviations, please consult Figure 1 of the main document.

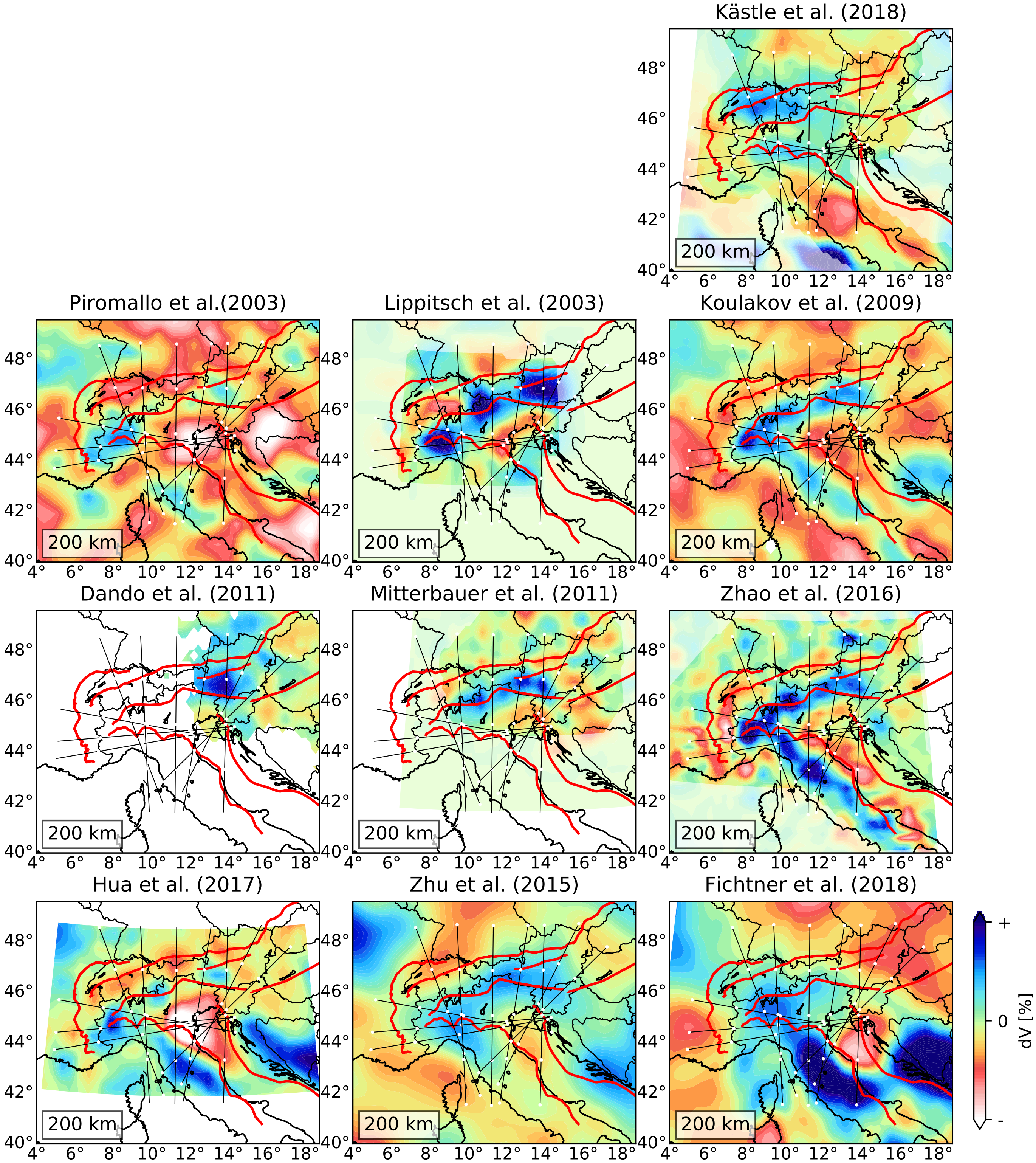

Figure S 2: Map comparison of different tomographic models at 200 km depth. The colors show either shear-velocity deviations (Zhu et al., 2015; Kästle et al., 2018; Fichtner et al., 2018) or compressional-velocity deviations (other models) from a regional starting model. The color scale is normalized to ±5% for Lippitsch et al. (2003); Zhu et al. (2015); Fichtner et al. (2018), ±4% for (Zhao et al., 2016), ±2.5 for Kästle et al. (2018) and ±3% for the other models. In most models, only central parts of the shown region are well resolved. Faults and tectonic limits (red lines) simplified from Schmid et al. (2004, 2008); Handy et al. (2010). Lighter colors indicate regions of lower resolution as defined in the original works. For an explanation of the abbreviations, please consult Figure 1 of the main document.

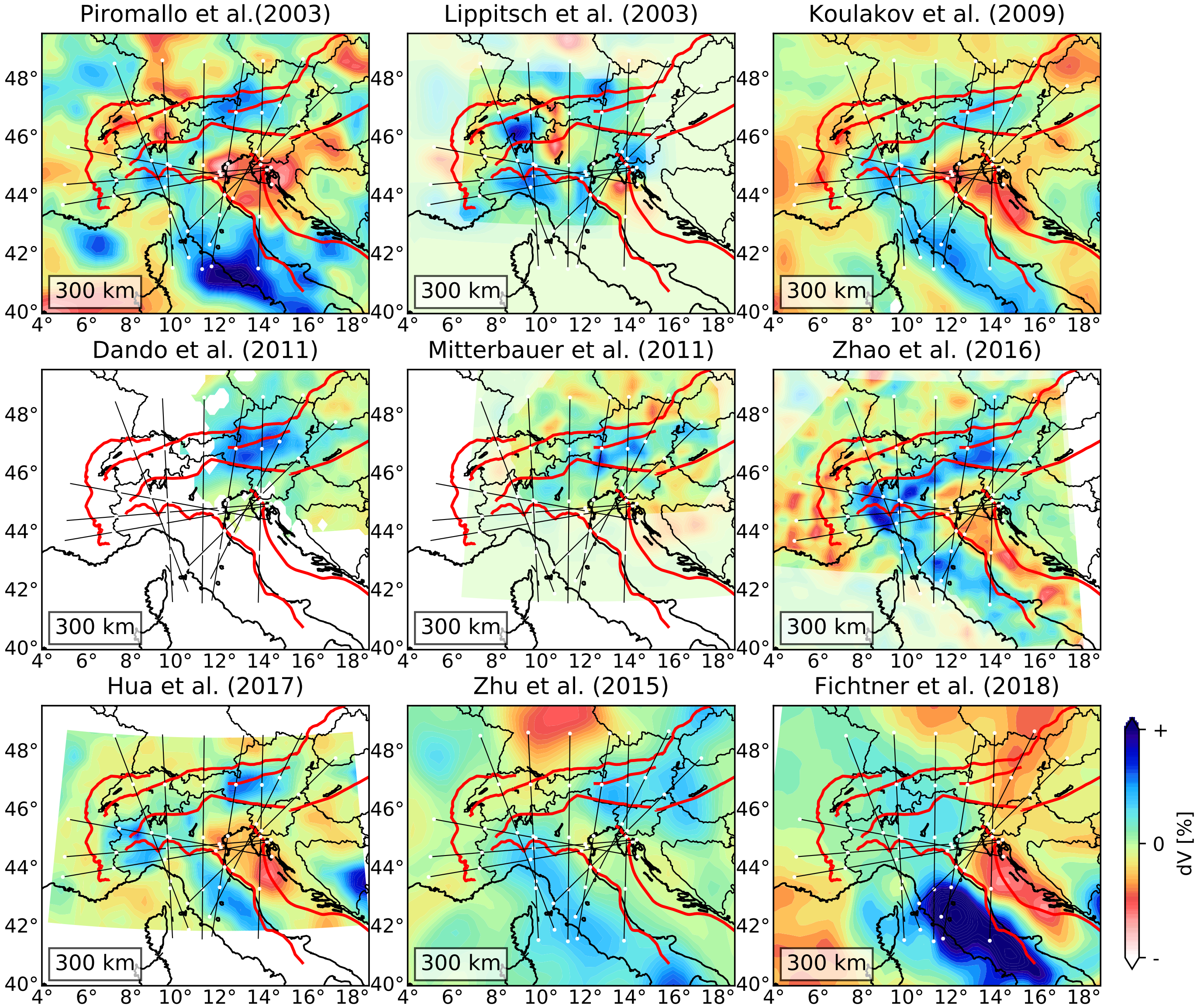

Figure S 3: Map comparison of different tomographic models at 300 km depth. The colors show either shear-velocity deviations (Zhu et al., 2015; Kästle et al., 2018; Fichtner et al., 2018) or compressional-velocity deviations (other models) from a regional starting model. The color scale is normalized to ±5% for Lippitsch et al. (2003); Zhu et al. (2015); Fichtner et al. (2018), ±4% for (Zhao et al., 2016) and ±3% for the other models. In most models, only central parts of the shown region are well resolved. Faults and tectonic limits (red lines) simplified from Schmid et al. (2004, 2008); Handy et al. (2010). Lighter colors indicate regions of lower resolution as defined in the original works. For an explanation of the abbreviations, please consult Figure 1 of the main document.

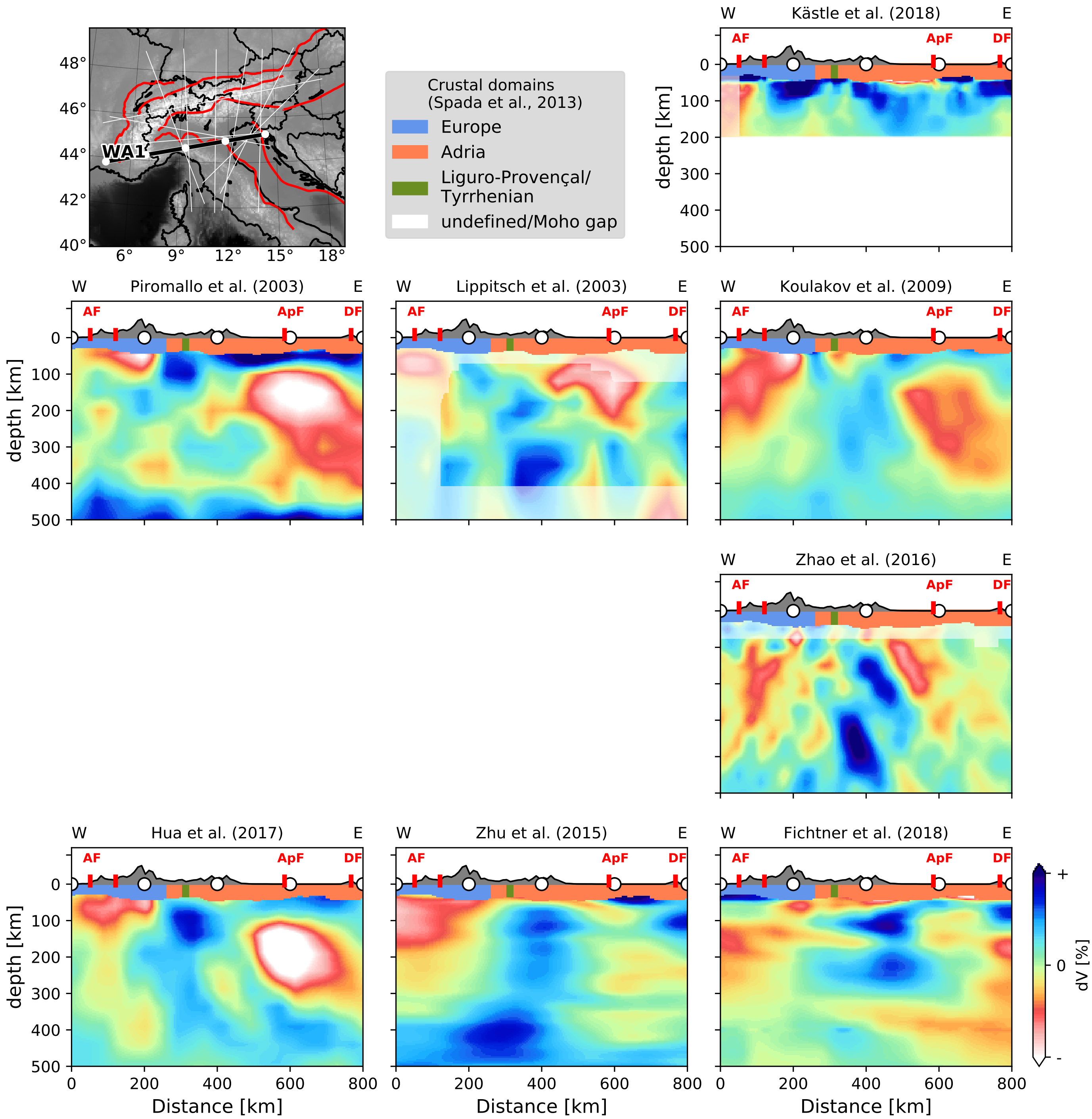

Figure S 4: Cross-section comparison of different tomographic models. Models that do not cover the crossed region are not shown. The colors show either shear-velocity deviations (Zhu et al., 2015; Kästle et al., 2018; Fichtner et al., 2018) or compressional-velocity deviations (other models) from a regional starting model. The color scale is normalized to ±5% for Lippitsch et al. (2003); Zhu et al. (2015); Fichtner et al. (2018), ±3% for (Zhao et al., 2016), ±2.5 for Kästle et al. (2018) and ±3% for the other models. Faults and tectonic limits (red lines in the map) simplified from Schmid et al. (2004, 2008); Handy et al. (2010). Lighter colors indicate regions of lower resolution as defined in the original works. For an explanation of the abbreviations, please consult Figure 1 of the main document.

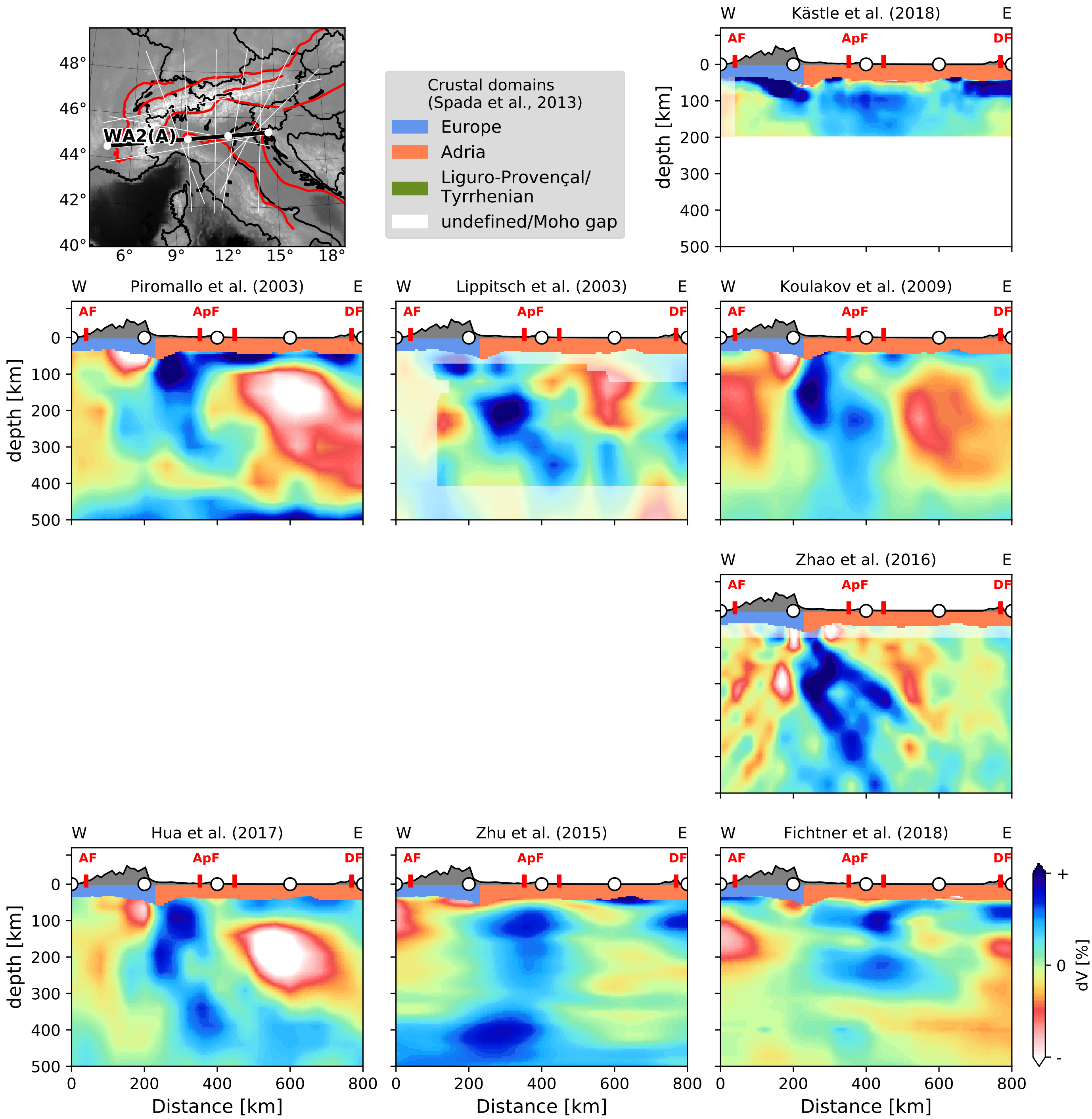

Figure S 5: Cross-section comparison of different tomographic models. Models that do not cover the crossed region are not shown. The colors show either shear-velocity deviations (Zhu et al., 2015; Kästle et al., 2018; Fichtner et al., 2018) or compressional-velocity deviations (other models) from a regional starting model. The color scale is normalized to ±5% for Lippitsch et al. (2003); Zhu et al. (2015); Fichtner et al. (2018), ±3% for (Zhao et al., 2016), ±2.5 for Kästle et al. (2018) and ±3% for the other models. Faults and tectonic limits (red lines in the map) simplified from Schmid et al. (2004, 2008); Handy et al. (2010). Lighter colors indicate regions of lower resolution as defined in the original works. For an explanation of the abbreviations, please consult Figure 1 of the main document.

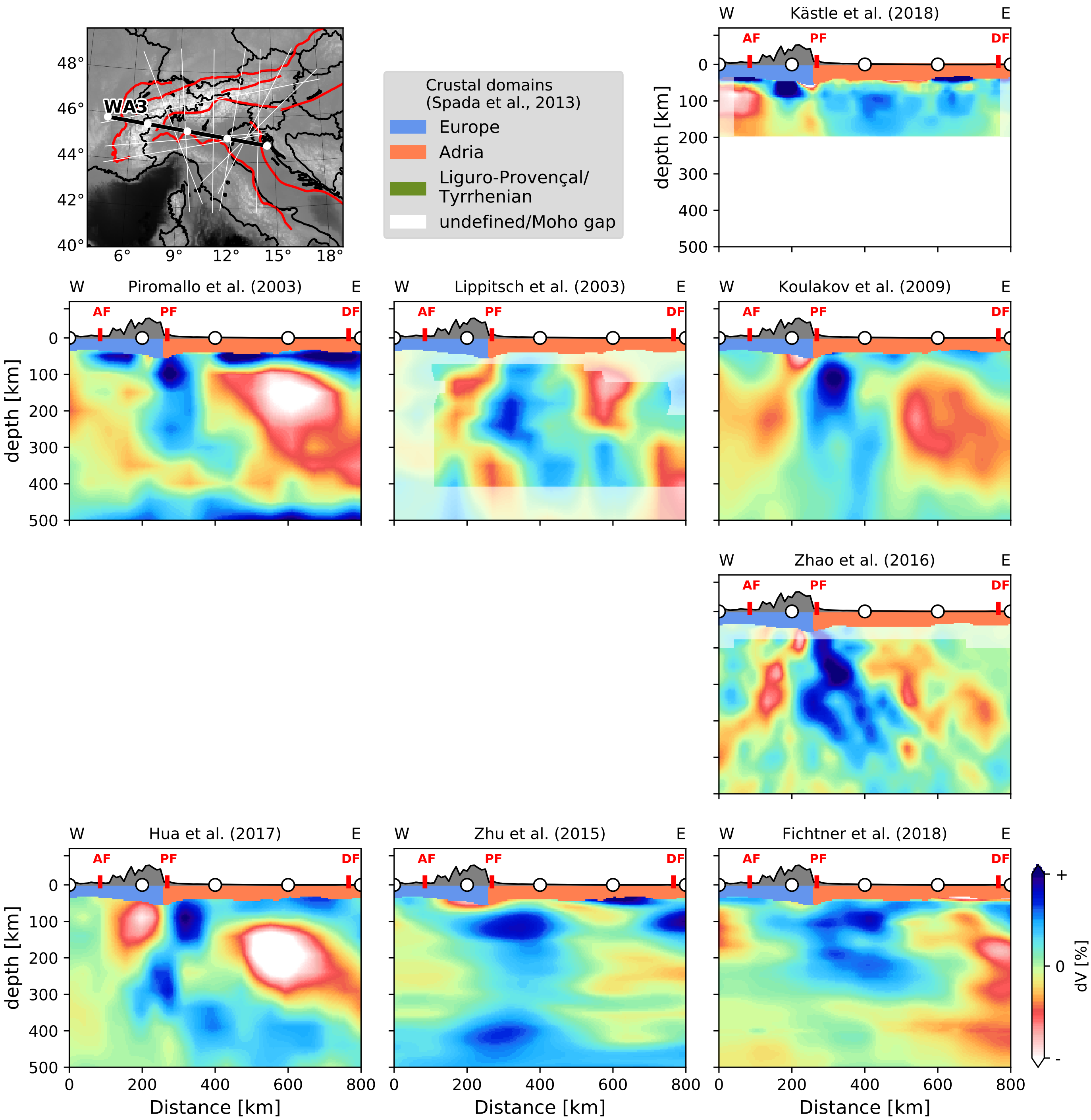

Figure S 6: Cross-section comparison of different tomographic models. Models that do not cover the crossed region are not shown. The colors show either shear-velocity deviations (Zhu et al., 2015; Kästle et al., 2018; Fichtner et al., 2018) or compressional-velocity deviations (other models) from a regional starting model. The color scale is normalized to ±5% for Lippitsch et al. (2003); Zhu et al. (2015); Fichtner et al. (2018), ±3% for (Zhao et al., 2016), ±2.5 for Kästle et al. (2018) and ±3% for the other models. Faults and tectonic limits (red lines in the map) simplified from Schmid et al. (2004, 2008); Handy et al. (2010). Lighter colors indicate regions of lower resolution as defined in the original works. For an explanation of the abbreviations, please consult Figure 1 of the main document.

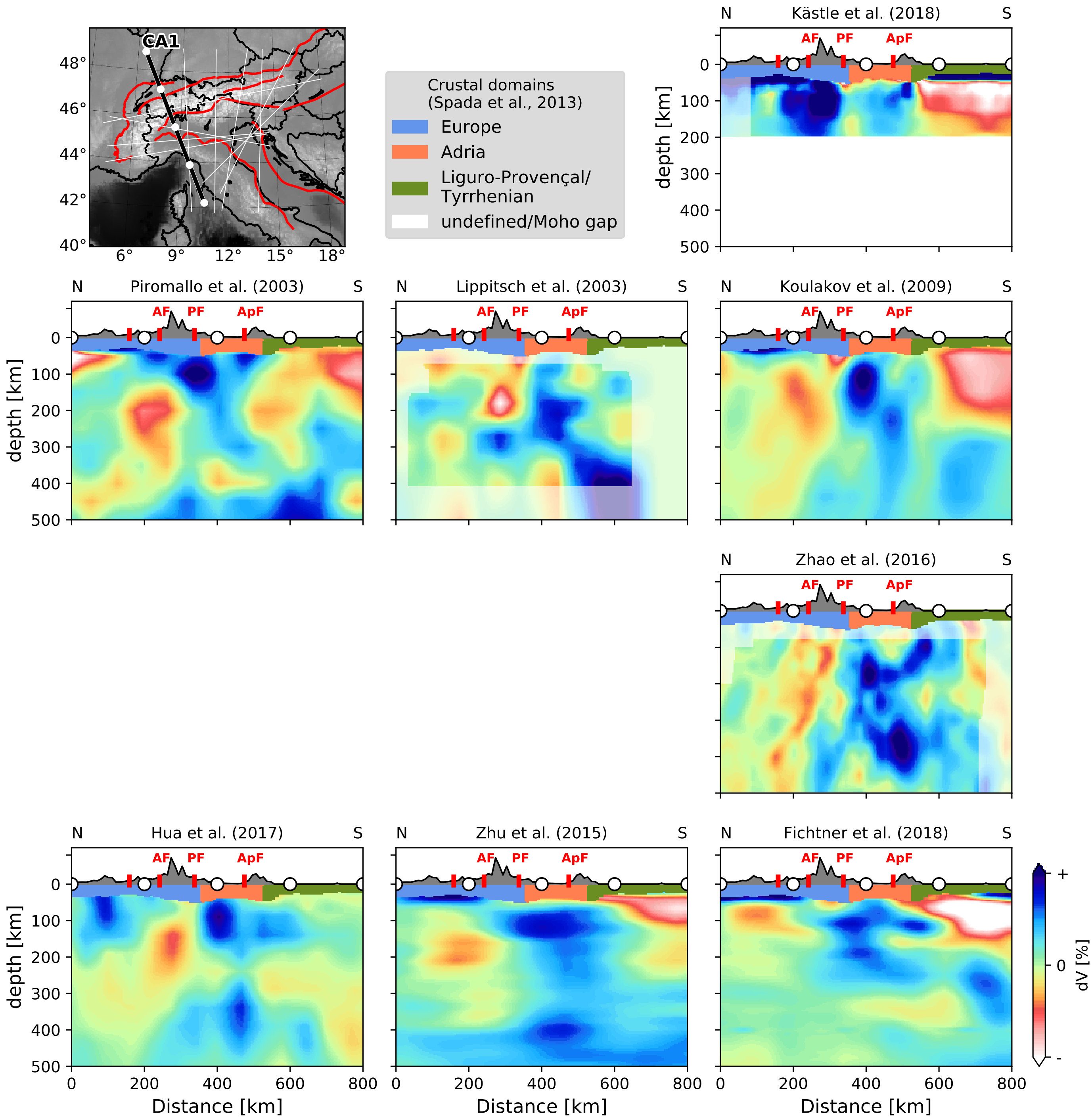

Figure S 7: Cross-section comparison of different tomographic models. Models that do not cover the crossed region are not shown. The colors show either shear-velocity deviations (Zhu et al., 2015; Kästle et al., 2018; Fichtner et al., 2018) or compressional-velocity deviations (other models) from a regional starting model. The color scale is normalized to ±5% for Lippitsch et al. (2003); Zhu et al. (2015); Fichtner et al. (2018), ±3% for (Zhao et al., 2016), ±2.5 for Kästle et al. (2018) and ±3% for the other models. Faults and tectonic limits (red lines in the map) simplified from Schmid et al. (2004, 2008); Handy et al. (2010). Lighter colors indicate regions of lower resolution as defined in the original works. For an explanation of the abbreviations, please consult Figure 1 of the main document.

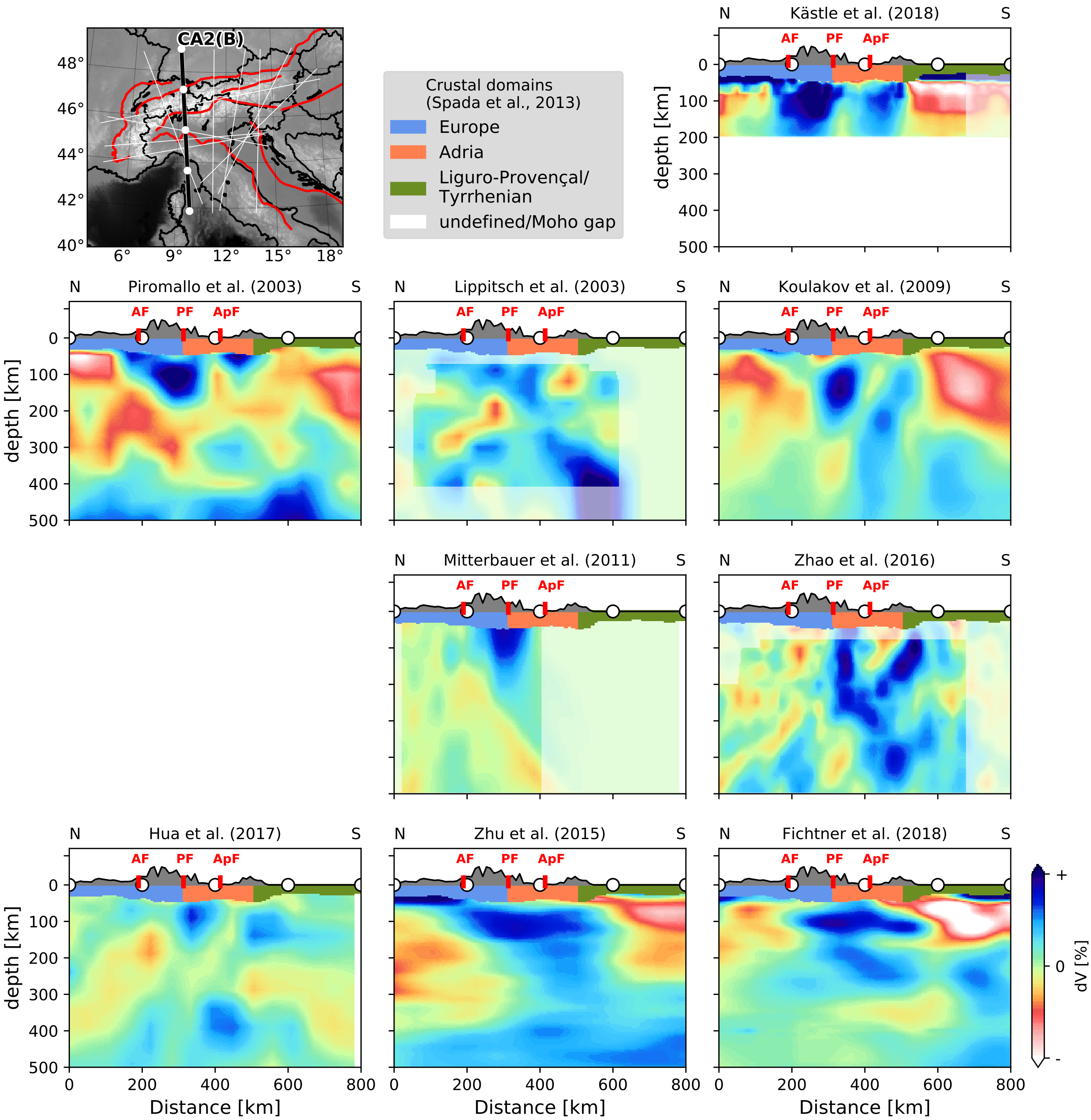

Figure S 8: Cross-section comparison of different tomographic models. Models that do not cover the crossed region are not shown. The colors show either shear-velocity deviations (Zhu et al., 2015; Kästle et al., 2018; Fichtner et al., 2018) or compressional-velocity deviations (other models) from a regional starting model. The color scale is normalized to ±5% for Lippitsch et al. (2003); Zhu et al. (2015); Fichtner et al. (2018), ±3% for (Zhao et al., 2016), ±2.5 for Kästle et al. (2018) and ±3% for the other models. Faults and tectonic limits (red lines in the map) simplified from Schmid et al. (2004, 2008); Handy et al. (2010). Lighter colors indicate regions of lower resolution as defined in the original works. For an explanation of the abbreviations, please consult Figure 1 of the main document.

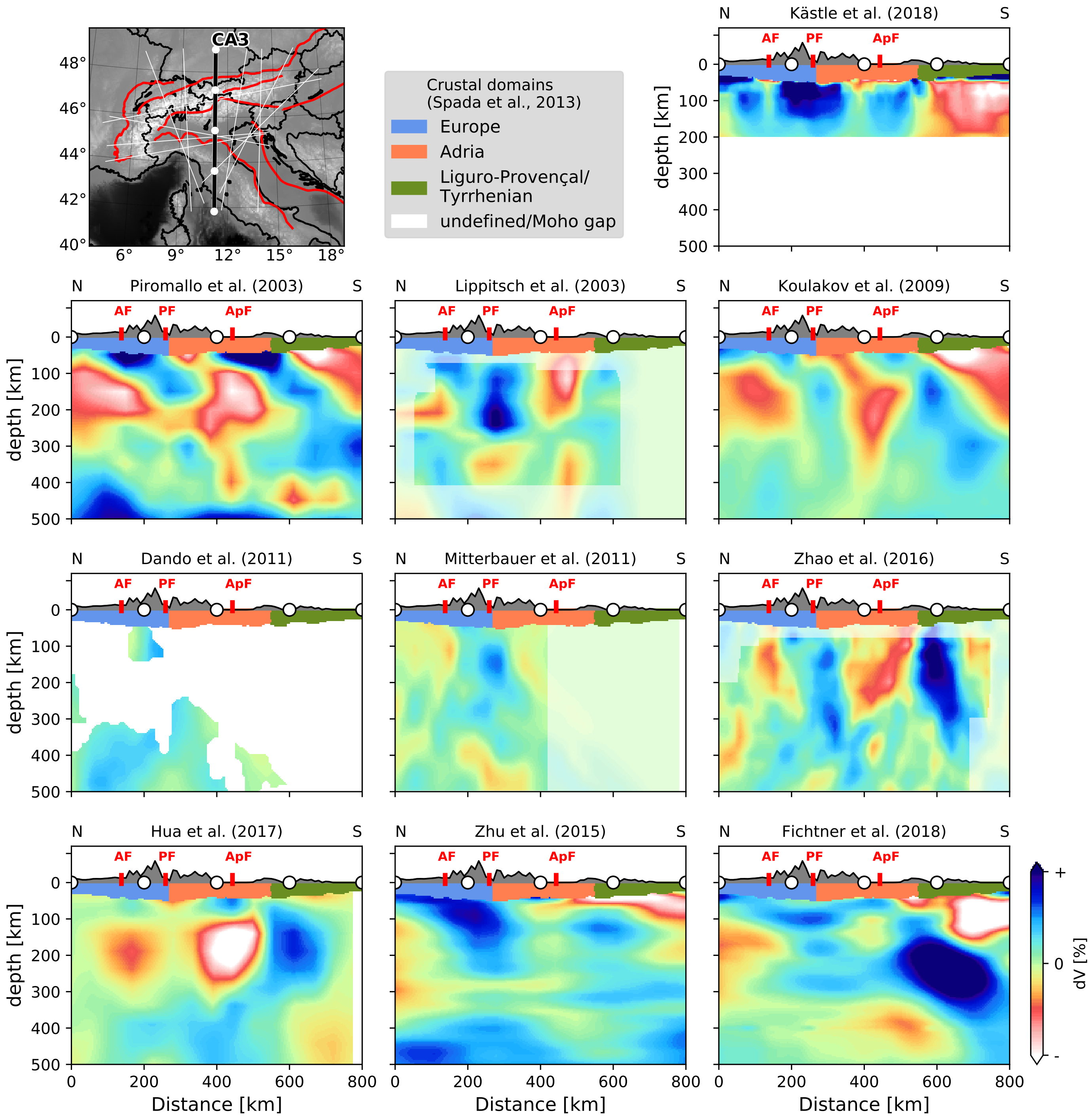

Figure S 9: Cross-section comparison of different tomographic models. Models that do not cover the crossed region are not shown. The colors show either shear-velocity deviations (Zhu et al., 2015; Kästle et al., 2018; Fichtner et al., 2018) or compressional-velocity deviations (other models) from a regional starting model. The color scale is normalized to ±5% for Lippitsch et al. (2003); Zhu et al. (2015); Fichtner et al. (2018), ±3% for (Zhao et al., 2016), ±2.5 for Kästle et al. (2018) and ±3% for the other models. Faults and tectonic limits (red lines in the map) simplified from Schmid et al. (2004, 2008); Handy et al. (2010). Lighter colors indicate regions of lower resolution as defined in the original works. For an explanation of the abbreviations, please consult Figure 1 of the main document.

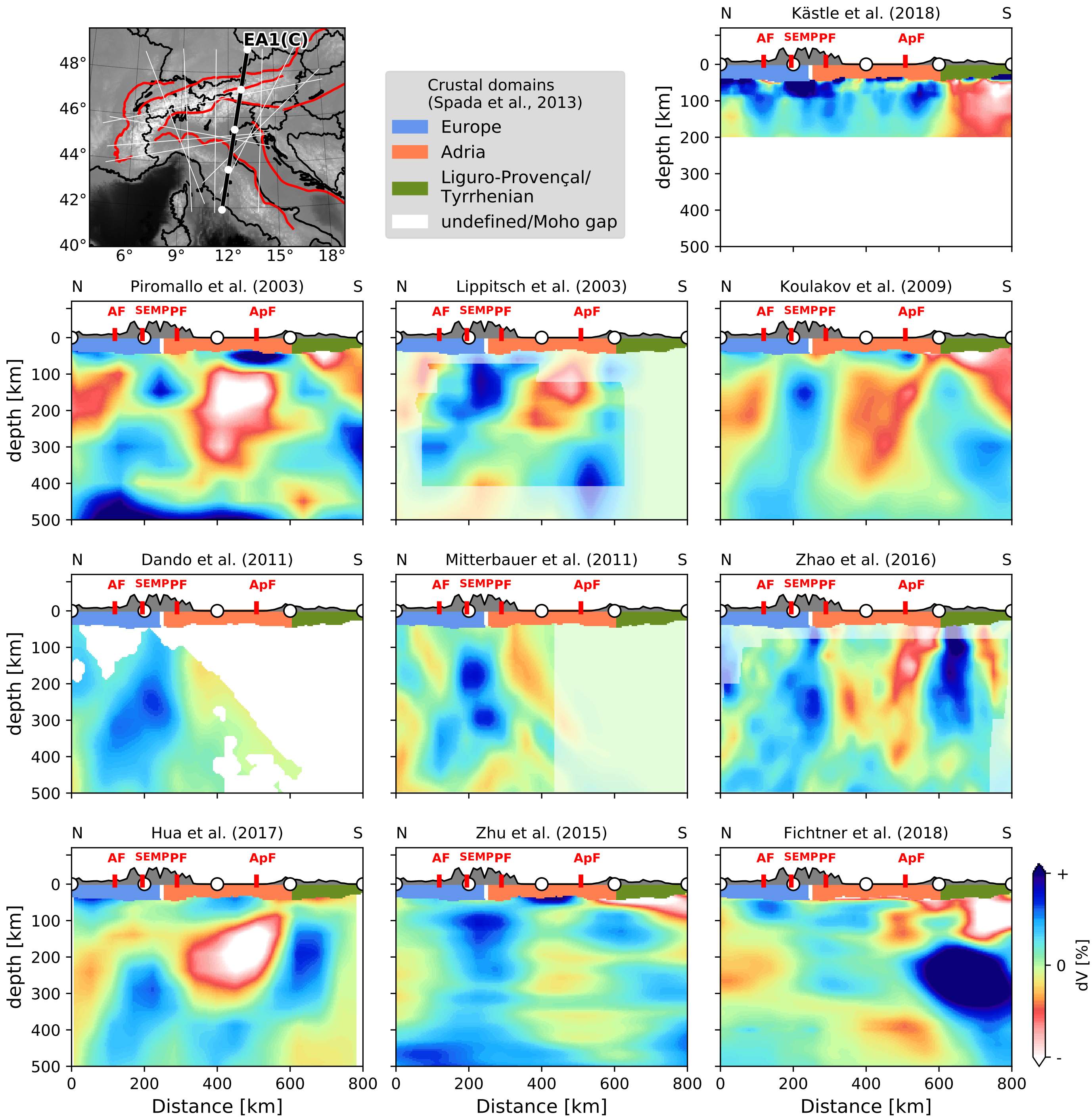

Figure S 10: Cross-section comparison of different tomographic models. Models that do not cover the crossed region are not shown. The colors show either shear-velocity deviations (Zhu et al., 2015; Kästle et al., 2018; Fichtner et al., 2018) or compressional-velocity deviations (other models) from a regional starting model. The color scale is normalized to ±5% for Lippitsch et al. (2003); Zhu et al. (2015); Fichtner et al. (2018), ±3% for (Zhao et al., 2016), ±2.5 for Kästle et al. (2018) and ±3% for the other models. Faults and tectonic limits (red lines in the map) simplified from Schmid et al. (2004, 2008); Handy et al. (2010). Lighter colors indicate regions of lower resolution as defined in the original works. For an explanation of the abbreviations, please consult Figure 1 of the main document.

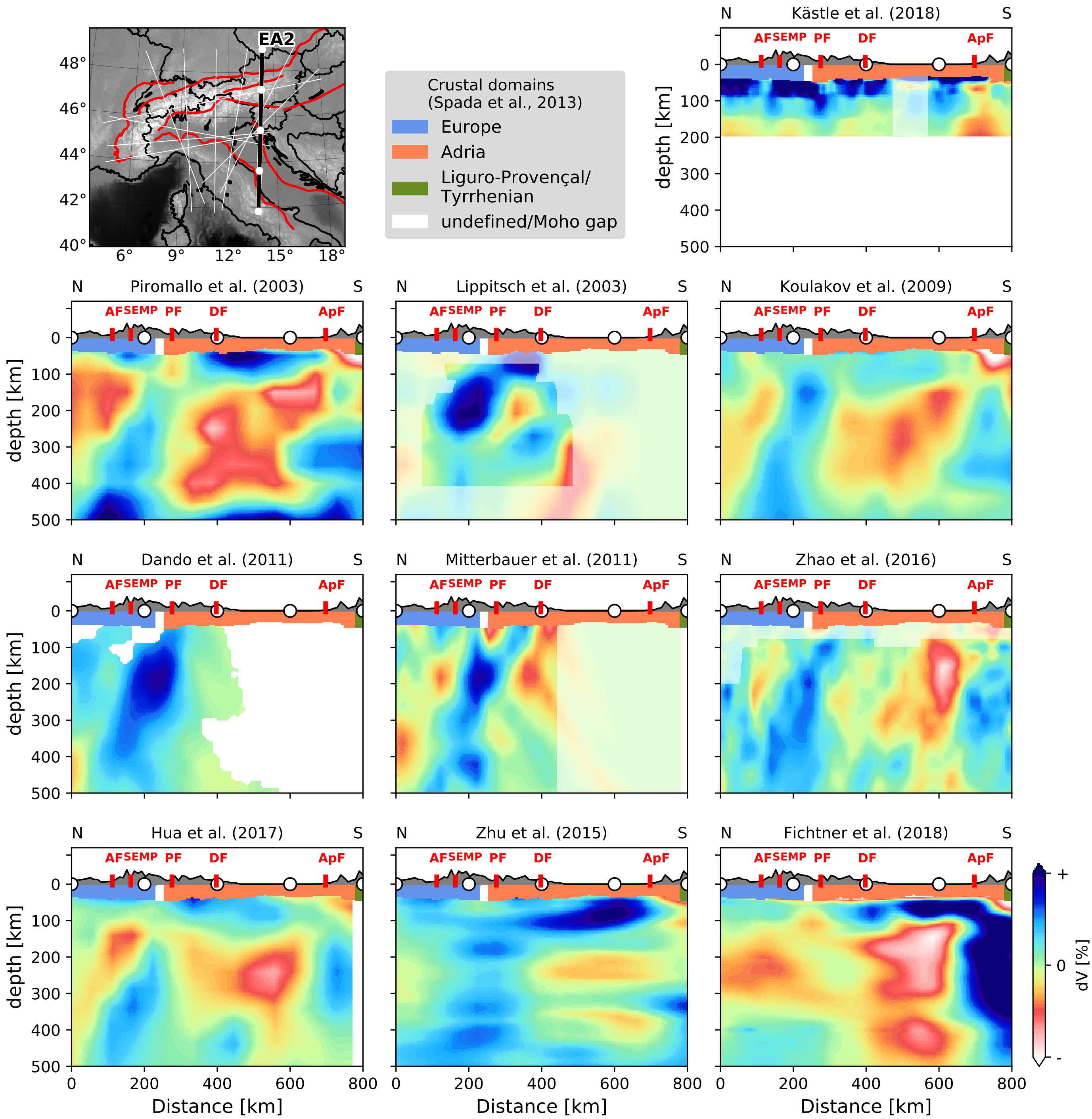

Figure S 11: Cross-section comparison of different tomographic models. Models that do not cover the crossed region are not shown. The colors show either shear-velocity deviations (Zhu et al., 2015; Kästle et al., 2018; Fichtner et al., 2018) or compressional-velocity deviations (other models) from a regional starting model. The color scale is normalized to ±5% for Lippitsch et al. (2003); Zhu et al. (2015); Fichtner et al. (2018), ±3% for (Zhao et al., 2016), ±2.5 for Kästle et al. (2018) and ±3% for the other models. Faults and tectonic limits (red lines in the map) simplified from Schmid et al. (2004, 2008); Handy et al. (2010). Lighter colors indicate regions of lower resolution as defined in the original works. For an explanation of the abbreviations, please consult Figure 1 of the main document.

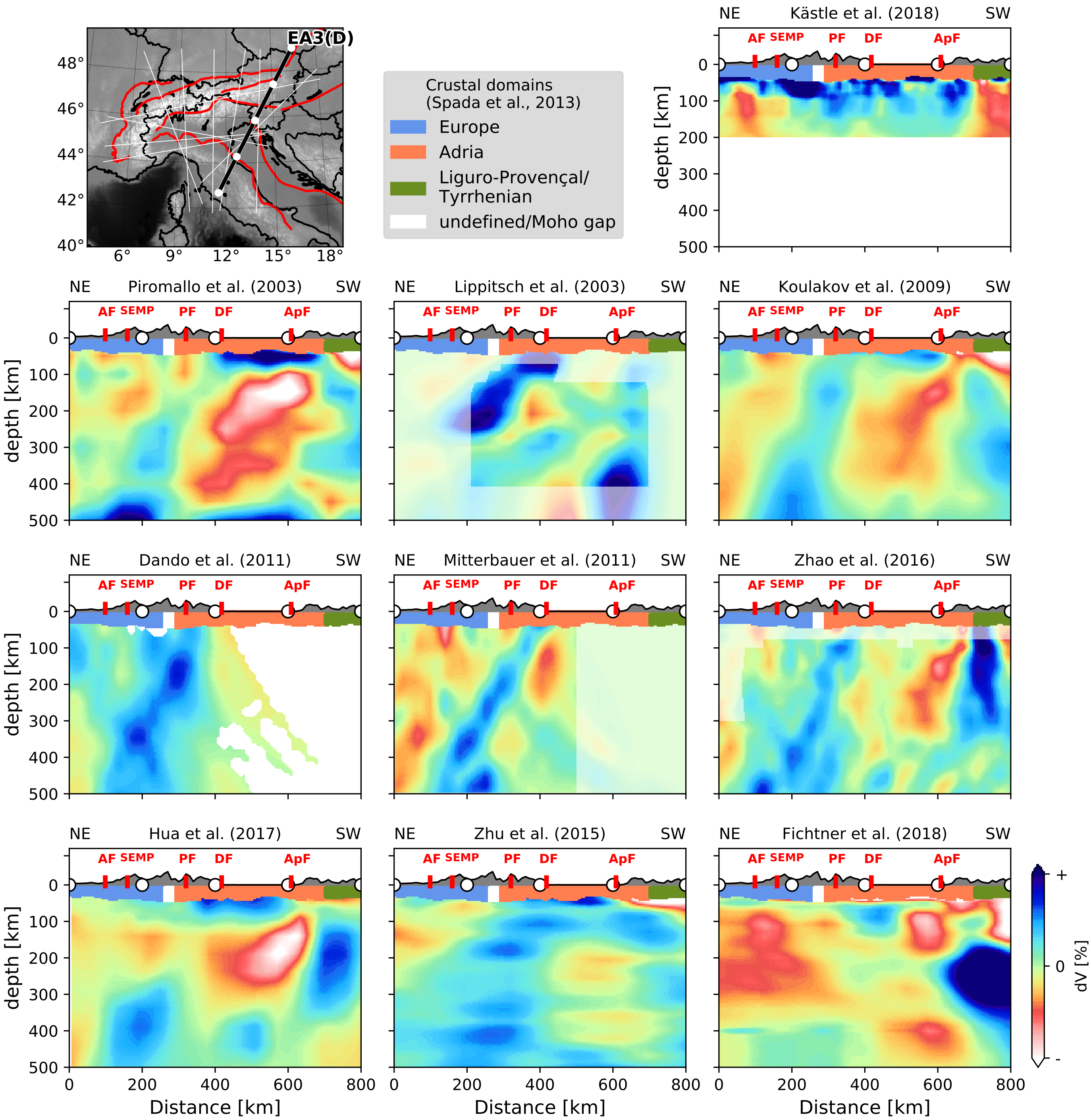

Figure S 12: Cross-section comparison of different tomographic models. Models that do not cover the crossed region are not shown. The colors show either shear-velocity deviations (Zhu et al., 2015; Kästle et al., 2018; Fichtner et al., 2018) or compressional-velocity deviations (other models) from a regional starting model. The color scale is normalized to ±5% for Lippitsch et al. (2003); Zhu et al. (2015); Fichtner et al. (2018), ±3% for (Zhao et al., 2016), ±2.5 for Kästle et al. (2018) and ±3% for the other models. Faults and tectonic limits (red lines in the map) simplified from Schmid et al. (2004, 2008); Handy et al. (2010). Lighter colors indicate regions of lower resolution as defined in the original works. For an explanation of the abbreviations, please consult Figure 1 of the main document.

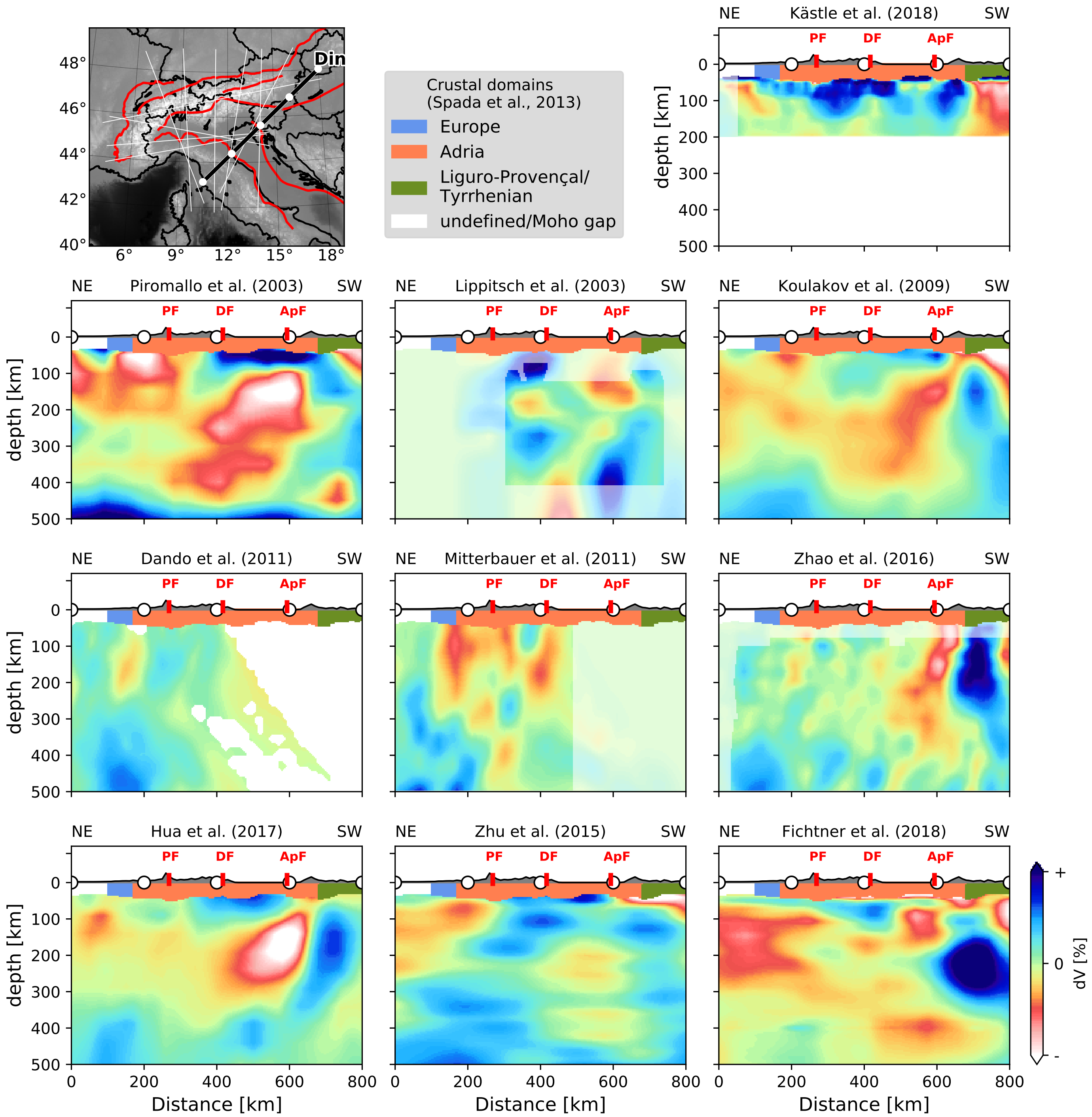

Figure S 13: Cross-section comparison of different tomographic models. Models that do not cover the crossed region are not shown. The colors show either shear-velocity deviations (Zhu et al., 2015; Kästle et al., 2018; Fichtner et al., 2018) or compressional-velocity deviations (other models) from a regional starting model. The color scale is normalized to ±5% for Lippitsch et al. (2003); Zhu et al. (2015); Fichtner et al. (2018), ±3% for (Zhao et al., 2016), ±2.5 for Kästle et al. (2018) and ±3% for the other models. Faults and tectonic limits (red lines in the map) simplified from Schmid et al. (2004, 2008); Handy et al. (2010). Lighter colors indicate regions of lower resolution as defined in the original works. For an explanation of the abbreviations, please consult Figure 1 of the main document.

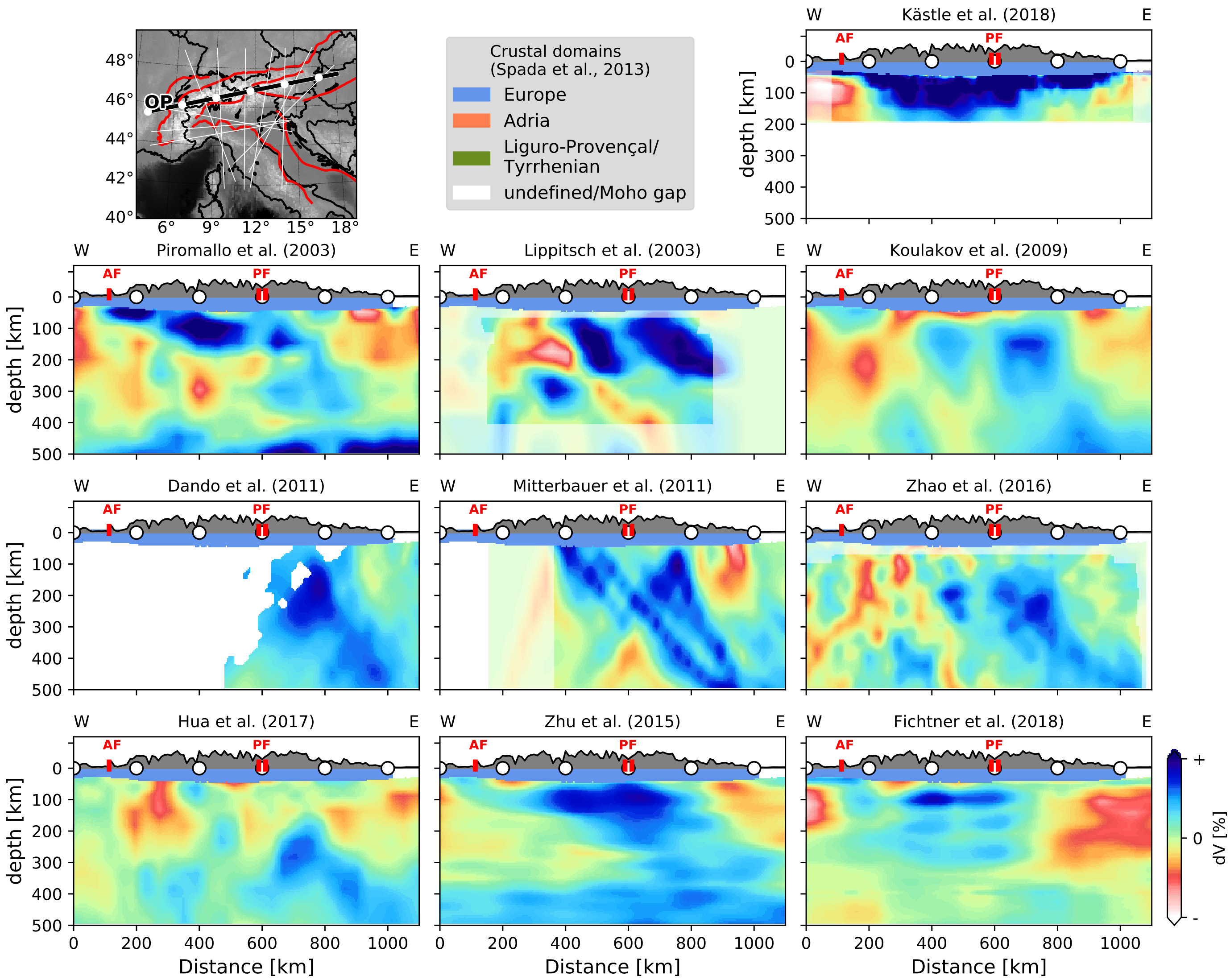

Figure S 14: Orogren-parallel (OP) cross-section comparison of different tomographic models. Models that do not cover the crossed region are not shown. The colors show either shear-velocity deviations (Zhu et al., 2015; Kästle et al., 2018; Fichtner et al., 2018) or compressional-velocity deviations (other models) from a regional starting model. The color scale is normalized to ±5% for Lippitsch et al. (2003); Zhu et al. (2015); Fichtner et al. (2018), ±3% for (Zhao et al., 2016), ±2.5 for Kästle et al. (2018) and ±3% for the other models. Faults and tectonic limits (red lines in the map) simplified from Schmid et al. (2004, 2008); Handy et al. (2010). Lighter colors indicate regions of lower resolution as defined in the original works. For an explanation of the abbreviations, please consult Figure 1 of the main document.

References

Brückl E (2011) *Lithospheric structure and tectonics of the eastern Alps-evidence from new seismic data* INTECH Open Access Publisher.

Dando B, Stuart G, Houseman G, Hegedüs E, Brückl E, Radovanović S (2011) Teleseismic tomography of the mantle in the Carpathian-Pannonian region of central Europe. *Geophys J Int* 186(1):11–31.

Fichtner A, van Herwaarden DP, Afanasiev M, Simutė S, Krischer L, Çubuk-Sabuncu Y, Taymaz T, Colli L, Saygin E, Villaseñor A, et al. (2018) The collaborative seismic earth model: generation 1. *Geophys Res Lett* 45(9):4007–4016.

Handy MR, Schmid SM, Bousquet R, Kissling E, Bernoulli D (2010) Reconciling plate-tectonic reconstructions of Alpine Tethys with the geological–geophysical record of spreading and subduction in the Alps. *Earth Sci Rev* 102(3):121–158.

Hetényi G, Plomerová J, Bianchi I, Exnerová HK, Bokelmann G, Handy MR, Babuška V, Group AEW, et al. (2018) From mountain summits to roots: Crustal structure of the Eastern Alps and Bohemian Massif along longitude 13.3 E. *Tectonophysics* 744:239–255.

Hua Y, Zhao D, Xu Y (2017) P-wave anisotropic tomography of the Alps. *J Geophys Res: Solid Earth* 122(6):4509-4528.

Kästle ED, El-Sharkawy A, Boschi L, Meier T, Rosenberg C, Bellahsen N, Cristiano L, Weidle C (2018) Surface Wave Tomography of the Alps Using Ambient-Noise and Earthquake Phase Velocity Measurements *J Geophys Res: Solid Earth*, 123(2):1770–1792.

Koulakov I, Kaban M, Tesauro M, Cloetingh S (2009) P-and S-velocity anomalies in the upper mantle beneath Europe from tomographic inversion of ISC data. *Geophys J Int* 179(1):345–366.

Kummerow J, Kind R, Oncken O, Giese P, Ryberg T, Wylegalla K, Scherbaum F, Group TW, et al. (2004) A natural and controlled source seismic profile through the Eastern Alps: TRANSALP *Earth Planet Sci Lett* 225(1):115–129.

Lippitsch R, Kissling E, Ansorge J. (2003) Upper mantle structure beneath the Alpine orogen from high-resolution teleseismic tomography. *J Geophys Res: Solid Earth*, 108(B8)

Mitterbauer U, Behm M, Brückl E, Lippitsch R, Guterch A, Keller GR, Koslovskaya E, Rumpfhuber EM, Šumanovac F (2011) Shape and origin of the East-Alpine slab constrained by the ALPASS teleseismic model. *Tectonophysics* 510(1):195–206.

Nussbaum C (2000) *Neogene tectonics and thermal maturity of sediments of the easternmost southern Alps (Friuli area, Italy)* PhD thesis.

Piromallo C, Morelli A (2003) P wave tomography of the mantle under the Alpine-Mediterranean area. *J Geophys Res: Solid Earth* 108(B2).

Schmid SM, Bernoulli D, Fügenschuh B, Matenco L, Schefer S, Schuster R, Tischler M, Ustaszewski K (2008) The Alpine-Carpathian-Dinaridic orogenic system: correlation and evolution of tectonic units. *Swiss J Geosci* 101(1):139–183.

Schmid SM, Fügenschuh B, Kissling E, Schuster R (2004) Tectonic map and overall architecture of the Alpine orogen. *Eclogae Geologicae Helvetiae* 97(1):93–117.

Schönborn G (1999) Balancing cross sections with kinematic constraints: the Dolomites (northern Italy) *Tectonics* 18(3):527–545.

Spada M, Bianchi I, Kissling E, Agostinetti NP, Wiemer S (2013) Combining controlled-source seismology and receiver function information to derive 3-D Moho topography for Italy. *Geophys J Int* 194(2):1050–1068.

Ustaszewski K, Schmid SM, Fügenschuh B, Tischler M, Kissling E, and Spakman, W. (2008) A map-view restoration of the Alpine-Carpathian-Dinaridic system for the Early Miocene. In *Swiss J Geosci*, 101(1):273-294.

Zhao L, Paul A, Malusà MG, Xu X, Zheng T, Solarino S, Guillot S, Schwartz S, Dumont T, Salimbeni S, et al. (2016) Continuity of the Alpine slab unraveled by high-resolution P wave tomography. *J Geophys Res: Solid Earth* 121(12):8720–8737.

Zhu H, Bozdağ E, Tromp J (2015) Seismic structure of the European upper mantle based on adjoint tomography *Geophys J Int* 201(1):18–52.